

25. J. Urbano *et al.*, *Organometallics* **24**, 1528 (2005).
 26. E. Despagnet-Ayoub *et al.*, *Organometallics* **27**, 4779 (2008).
 27. J. Urbano *et al.*, *Organometallics* **28**, 5968 (2009).
 28. J. M. DeSimone, E. Tumas, Eds., *Green Chemistry Using Liquid and Supercritical Carbon Dioxide* (Oxford Univ. Press, Oxford, 2003).
 29. Materials and methods are available as supporting material on *Science* Online.
 30. M. P. Doyle, M. A. McKervey, T. Ye, *Modern Catalytic Methods for Organic Synthesis with Diazo Compounds* (Wiley, New York, 1998).
 31. A. Caballero, A. Prieto, M. M. Diaz-Requejo, P. J. Pérez, *Eur. J. Inorg. Chem.* **2009**, 1137 (2009).
 32. S. J. Blanksby, G. B. Ellison, *Acc. Chem. Res.* **36**, 255 (2003).
 33. E. Nakamura, N. Yoshikai, M. Yamanaka, *J. Am. Chem. Soc.* **124**, 7181 (2002).
 34. A. A. C. Braga *et al.*, *Organometallics* **25**, 5292 (2006).

35. A reviewer mentioned the possibility of the involvement of radical species. Extensive previous work favors the metallocarbene route [see (19) and references therein]. Moreover, these experiments were carried out in a vessel that was neither purged nor vented; therefore, 100 mL of air was present in the reaction mixture. The oxygen contained in that volume would preclude the conversion of any radical into the desired product. See (36).

36. G. Asensio, R. Mello, M. E. González-Núñez, C. Boix, J. Royo, *Tetrahedron Lett.* **38**, 2373 (1997).

Acknowledgments: We dedicate this work to Professor Ernesto Carmona. Support for this work was provided by the Ministerio de Ciencia e Innovación (grants CTQ2008-00042-BQU, CTQ2007-65251-BQU, and CTQ2007-30762-E), the European Research Area Chemistry Programme (2nd call "Chemical activation of carbon dioxide and methane" contract no. 1736154), the Consolider Ingenio 2010 (grants CSD2006-003 and

CSD2007-00006), the Institut de Chimie of the CNRS, the Junta de Andalucía (P07-FQM-2870), and the Generalitat Valenciana (ACOMP/2010/155). We thank the Servicio Central de Soporte a la Investigación Experimental (Universidad de Valencia) for access to the instrumental facilities and J. de la Rosa and A. Sánchez de la Campa (Universidad de Huelva) for ICP-MS analyses.

Supporting Online Material

www.sciencemag.org/cgi/content/full/332/6031/835/DC1
 Materials and Methods

SOM Text

Figs. S1 to S7

Tables S1 and S2

References 25, 26, and 37

10 February 2011; accepted 19 March 2011
 10.1126/science.1204131

Massive CO₂ Ice Deposits Sequestered in the South Polar Layered Deposits of Mars

Roger J. Phillips,^{1*} Brian J. Davis,^{2†} Kenneth L. Tanaka,³ Shane Byrne,⁴ Michael T. Mellon,⁵ Nathaniel E. Putzig,² Robert M. Haberle,⁶ Melinda A. Kahre,⁷ Bruce A. Campbell,⁸ Lynn M. Carter,⁹ Isaac B. Smith,¹⁰ John W. Holt,¹⁰ Suzanne E. Smrekar,¹¹ Daniel C. Nunes,¹¹ Jeffrey J. Plaut,¹¹ Anthony F. Egan,¹² Timothy N. Titus,³ Roberto Seu¹³

Shallow Radar soundings from the Mars Reconnaissance Orbiter reveal a buried deposit of carbon dioxide (CO₂) ice within the south polar layered deposits of Mars with a volume of 9500 to 12,500 cubic kilometers, about 30 times that previously estimated for the south pole residual cap. The deposit occurs within a stratigraphic unit that is uniquely marked by collapse features and other evidence of interior CO₂ volatile release. If released into the atmosphere at times of high obliquity, the CO₂ reservoir would increase the atmospheric mass by up to 80%, leading to more frequent and intense dust storms and to more regions where liquid water could persist without boiling.

The martian atmosphere is dominated by CO₂ with an annual mean pressure currently about 6 mbar (6 hPa) (1), although

early in the planet's history CO₂ likely existed at the ~1 bar level. Some of this ancient atmospheric CO₂ may be stored in the polar layered deposits (PLD) (2), although, it is now thought, only in modest quantities. The water-ice-dominated

southern PLD (SPLD) presently host a small [<5 -m thick, ~90,000 km² (3)] perennial CO₂-ice deposit (4) overlying a thin water-ice layer (5), which together compose the south pole residual cap (SPRC). If the SPRC CO₂ material were to be released completely into the atmosphere, the increase in pressure would be only a few tenths of a mbar and insufficient to buffer the atmospheric CO₂ during changing climatic conditions (5). Here, we use radar-sounder data to show that the volume of sequestered CO₂ in the SPLD is substantially larger than previously believed, competing in magnitude with the present atmospheric abundance.

SHARAD (Shallow Radar) is a sounding radar on the Mars Reconnaissance Orbiter (MRO) mission (6), and its results are displayed in radar-grams with axes of time delay and orbital position (Fig. 1). Previous mapping of subsurface reflectors by SHARAD in the north PLD (NPLD) revealed a crisp radar stratigraphy to the base of the deposits (7, 8). For the SPLD, the radar signal does not penetrate the deposits as deeply as in the NPLD, and in only a limited number of places is there a well-defined stratigraphy (9). There are some regions with nearly reflection-

¹Planetary Science Directorate, Southwest Research Institute, Boulder, CO 80302, USA and Department of Earth and Planetary Sciences, Washington University, St. Louis, MO 63130, USA. ²Department of Space Studies, Southwest Research Institute, Boulder, CO 80302, USA. ³Astrogeology Science Center, U.S. Geological Survey, Flagstaff, AZ 86001, USA. ⁴Lunar and Planetary Laboratory, University of Arizona, Tucson, AZ 85721, USA. ⁵Laboratory for Atmospheric and Space Physics, University of Colorado, Boulder, CO 80303, USA. ⁶Space Science and Astrobiology Division, National Aeronautics and Space Administration (NASA) Ames Research Center, Moffett Field, CA 94035, USA. ⁷Bay Area Environmental Research Institute/NASA Ames Research Center, Moffett Field, CA 94035, USA. ⁸Center for Earth and Planetary Studies, Smithsonian Institution, Washington, DC 20013, USA. ⁹Science and Exploration Directorate, NASA Goddard Space Flight Center, Greenbelt, MD 20771, USA. ¹⁰Institute for Geophysics, Jackson School of Geosciences, University of Texas, Austin, TX 78758, USA. ¹¹Jet Propulsion Laboratory, California Institute of Technology, Pasadena, CA 91109, USA. ¹²Department of Space Operations, Southwest Research Institute, Boulder, CO 80302, USA. ¹³Department of Information Engineering, Electronics and Telecommunications, Sapienza University of Rome, 18-00184 Rome, Italy.

*To whom correspondence should be addressed. E-mail: roger@boulder.swri.edu

†Present address: Department of Geophysics, Colorado School of Mines, Golden, CO 80401, USA.

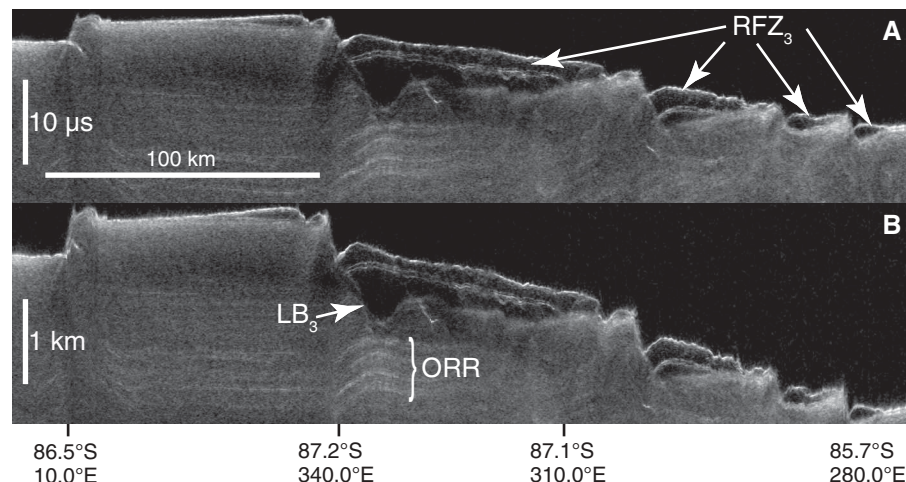


Fig. 1. SHARAD radargram 5968-01 traversing RFZ₃ terrain shown in original time-delay format (A) and converted to depth (B) by using the permittivity of water ice. Ground track location is shown in Fig. 3. ORR and LB₃ are indicated.

free subsurface zones (RFZ) extending downward from near the surface to depths approaching 1 km (fig. S1). The RFZs can be subdivided into four distinct types and locations (table S1) on the basis of their radar characteristics; here, we focus on RFZ₃, which is spatially coincident with the SPRC. Except for a commonly occurring thin layer that bisects the unit (Fig. 1), RFZ₃ is the most reflection-free volume that we have seen on Mars with SHARAD data: the signal level within approaches the background noise. Deeper reflectors passing beneath RFZ₃ brighten slightly more than expected on the basis of the change in thickness of typical SPLD material, implying that RFZ₃ deposits attenuate a radar signal less severely than these typical regions. Importantly, the low-power RFZ₃ radar return is thus not caused by strong scattering or absorption losses within the deposit.

To determine the real permittivity (ϵ') of RFZ₃, we mapped key SHARAD reflectors for 79 MRO orbits (fig. S2). The lower boundary of RFZ₃, LB₃, is a highly irregular buried erosional

surface that truncates subhorizontal reflectors. Extending several hundred meters beneath RFZ₃ is a zone of unorganized, weak radar reflectors that in turn is underlain by a coherent sequence of organized (layered) radar reflectors (ORR). By using the a priori assumption of a bulk water-ice composition ($\epsilon' = 3.15$) for the SPLD, we converted the vertical axis of radargrams from time delay to depth. The converted ORR sequence beneath LB₃ is typically offset from surrounding regions and exhibits significant topographic variations (Fig. 1B) that are strongly anticorrelated with LB₃ (Fig. 2A). This anticorrelation is unexpected because there is very likely no geological link between the earlier deposition of the ORR and the later erosion of the material above it that was subsequently filled with RFZ₃ material [see (10) for details]. On the basis of the argument that the anticorrelations are the fortuitous result of an incorrect choice of ϵ' for RFZ₃, we found for each radargram the ϵ' value that gave zero correlation between LB₃ and a test reflector (TR) in the ORR sequence (Fig. 2,

B and C) (10). A second method (10) sought to minimize topographic perturbations and offsets on the TR by finding the ϵ' value that obtained the smallest residuals to a linear regression on this interface (Fig. 2, D and E). Both methods tended to produce a relatively smooth and subhorizontal disposition to the TR, similar in nature to the likely extension of ORR observed by SHARAD in the Promethei Lingula region (9). Forty-one of the 79 radargrams were suitable for quantitative analyses using these procedures, and by using different strategies we found mean values for ϵ' of the RFZ₃ volume in the range of 2.0 to 2.2, with standard deviations of 0.1 to 0.2 (10).

These permittivity estimates for RFZ₃ are unexpectedly close to a laboratory-measured value of low-porosity CO₂ ice of 2.12 ± 0.04 (11), similar to the well-known frequency-independent value of about 2.2 for bulk dry ice (12). The SHARAD-derived permittivity values are substantially lower than those of water ice (3.15) and CO₂ clathrate-hydrate ice (~2.85) (13), strongly supporting the hypothesis that RFZ₃ is a solid CO₂ deposit. An alternative view that RFZ₃ is porous water ice can be rejected on the basis of permittivity-thickness relationships (10).

With the permittivities estimated, we converted the time delays through RFZ₃ (using $\epsilon' = 2.1$) to thicknesses over each of the 79 radar traverses (fig. S3) and by interpolation constructed a continuous thickness distribution. Figure 3 shows this result placed over a geological map showing stratigraphic units in a portion of the SPLD (14, 15). Of interest here are the largely overlapping horizontal extents of the AA₃ unit and the successively overlying water-ice (AA_{4a}) and CO₂-ice (AA_{4b}) units making up the SPRC. Also shown are the contacts (dashed) for unit AA₃, with the locations constrained well by exposures in troughs and by partial exposures beneath the SPRC. Where SHARAD data are available, there is a remarkable spatial correlation of RFZ₃ to the AA₃ unit except for the extremes of northward-extending lobes of the unit (16). Thus, we propose that the AA₃ unit is in fact RFZ₃, and its composition is dominated by CO₂ ice.

The AA₃ unit contains a system of large troughs, up to several km wide and typically <100 m deep, that do not cut older units (Fig. 3). In turn, smaller parallel aligned ridges, troughs, and elongate depressions mark some of these large troughs, and in places the depressions appear as coalescing or elongated pits (Fig. 4). Additionally, the westernmost outcrops of unit AA₃ (north of 87°S and near 240° to 270°E) include about 20 rimless circular pits (~300- to ~4000-m diameter), which do not occur in layers underlying unit AA₃ and do not display any rims or ejecta. All of these smaller troughs, depressions, and pits appear to result from erosion and removal of unit AA₃, with a strong component of sublimation and collapse. These features are not found elsewhere in the SPLD, and the CO₂-ice layer (AA_{4b}) of the SPRC is the only other perennial

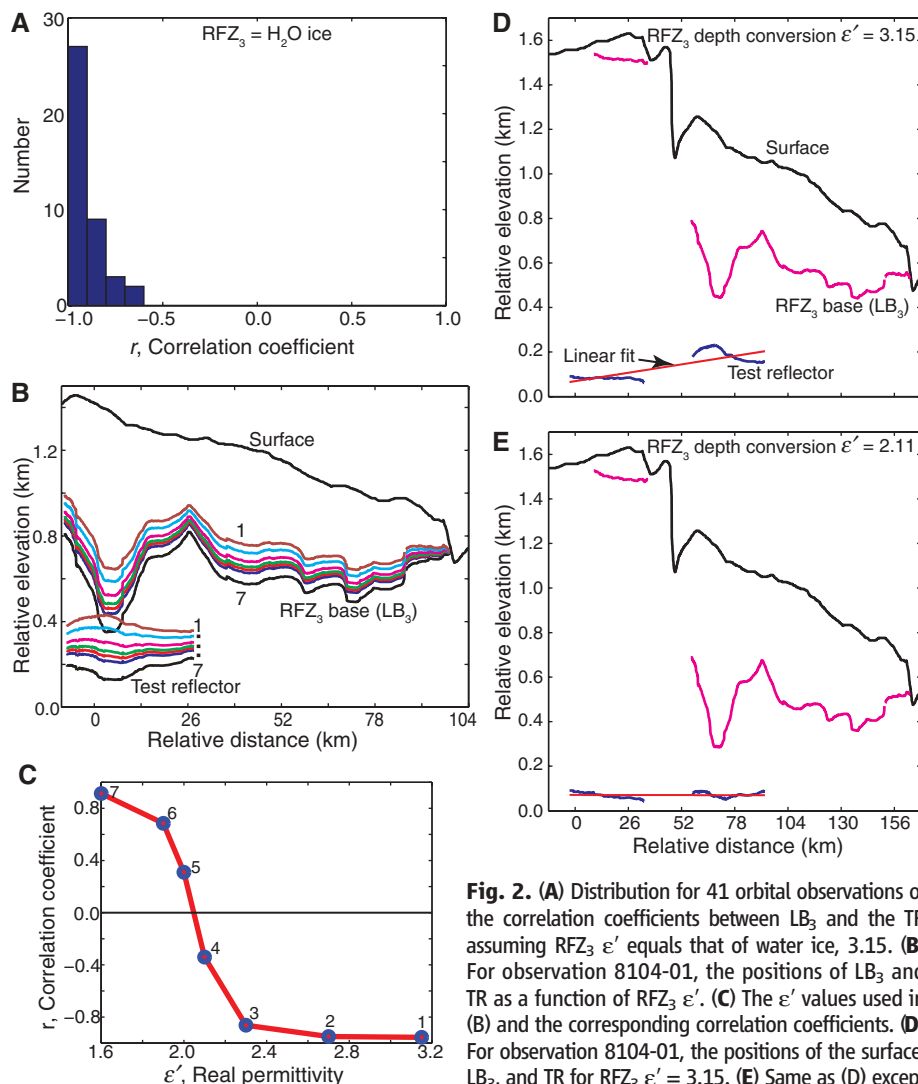


Fig. 2. (A) Distribution for 41 orbital observations of the correlation coefficients between LB₃ and the TR assuming RFZ₃ ϵ' equals that of water ice, 3.15. (B) For observation 8104-01, the positions of LB₃ and TR as a function of RFZ₃ ϵ' . (C) The ϵ' values used in (B) and the corresponding correlation coefficients. (D) For observation 8104-01, the positions of the surface, LB₃, and TR for RFZ₃ $\epsilon' = 3.15$. (E) Same as (D) except RFZ₃ $\epsilon' = 2.11$, which gives the best-fitting linear regression on TR.

Fig. 3. Polar stereographic map of a portion of the SPLD, showing RFZ₃ thickness variations interpolated to a continuous volume for the 79 SHARAD ground tracks where RFZ₃ deposits were observed. Bright colors indicate deposit thicknesses calculated by using $\epsilon' = 2.1$, and the histogram (inset) provides their relative occurrences. Base map (subdued colors) shows SPLD stratigraphy (14, 15) with geologic units from oldest to youngest: HNu (substrate underlying SPLD); AA₁ (evenly bedded layers, up to 3.5 km thick); AA₂ (evenly bedded layers, <300 m thick); AA₃ (~300 m thick); and AA_{4a} and AA_{4b} (water-ice and CO₂-ice members, respectively, of the SPRC). The units are separated by unconformities, indicating episodes of erosion between them that resulted in retreat of the original lateral extents of the units and in development of local troughs and depressions. Dashed lines indicate boundary lines of unit AA₃ where partially buried. Mars Orbiter Laser Altimeter (MOLA) shaded relief base at 115 m per pixel; because of spacecraft orbital inclinations, no SHARAD or MOLA data are available poleward of ~87°S. Ground track of observation 5968-01 (Fig. 1) is shown.

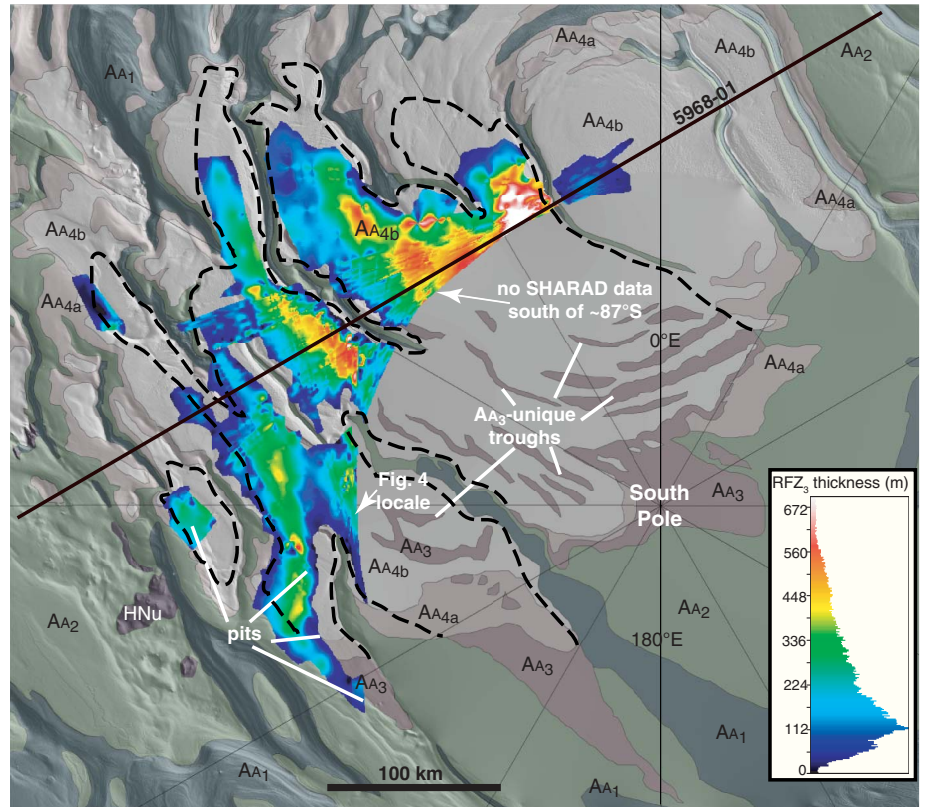
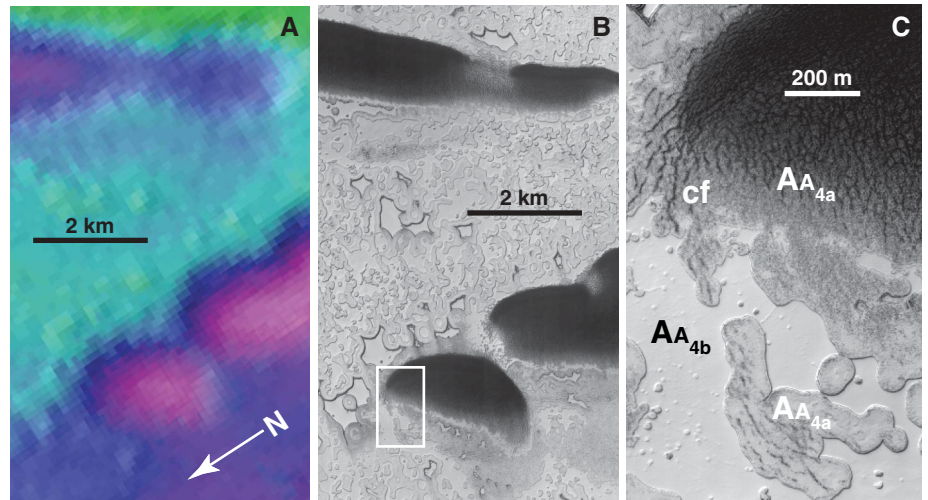


Fig. 4. MOLA topographic image (A) in the vicinity of 87°S, 268°E, showing linear depressions or troughs in the AA₃ unit. The total elevation range of the image is ~75 m from the lowest (pink) to the highest (green) surface. The troughs are associated with circular pits (B), part of MRO HiRISE (High Resolution Imaging Science Experiment) image ESP_014342_0930] and are thinly buried by the SPRC (C), with unit AA_{4b} (CO₂ ice) displaying sublimation windows into a fractured water-ice unit AA_{4a} beneath (northwestern corner of a pit). The water-ice layer is completely exposed in the northeastern portion of this pit, where intense polygonal fracturing gives way to concentric fracturing on the pit rim (cf).



unit in the SPLD that exhibits clear (although different) morphological indicators of sublimation (5). The lack of sublimation features in exposures of the older units AA₁ and AA₂ indicate that CO₂, and not H₂O, is the sublimating material in the AA₃ unit, as might be expected given their relative volatilities. The AA₃ unit with pits distributed along the linear depressions is covered by a heavily fractured SPRC water-ice layer (AA_{4a}) that is overlain in places by the sublimating SPRC CO₂ layer (AA_{4b}) that formed after the fracturing (Fig. 4). The fracturing, not found in other SPLD units, may be a response to continuing unit AA₃ sublimation after the pits had first formed. The other three RFZs lack surface expressions of sublimation, but nondetection of

sufficiently rugged lower boundaries precluded permittivity estimates.

Because we equate RFZ₃ to unit AA₃, we used the areal distribution of the geological unit to extrapolate the RFZ₃ volume poleward of ~87°S, achieving a total volume range (17) of ~9500 to 12,500 km³ (10). In contrast, the volume of the CO₂-dominated SPRC is less than 380 km³ (3), about 30 times less. The RFZ₃ thickness-independent permittivity values (10) imply a density close to that of bulk dry ice, 1500 to 1600 kg m⁻³ (18), which converts volume to an equivalent atmospheric pressure of 4 to 5 mbar, up to ~80% of the equivalent mass in the current atmosphere. The collapse features in the AA₃ unit suggest that the RFZ₃ mass has been waning, and

an isolated patch of RFZ₃ (at ~345°E in Figs. 1 and 3) appears to be an erosional remnant. This suggests that the atmosphere has contained less than the present ~6 mbar of CO₂, hinting at past atmospheric collapse.

The lack of reflections in RFZ₃ apart from the bisecting layer can be interpreted as a lack of dust (7). Global climate models (GCMs) suggest (19) that, when the obliquity of Mars drops below a critical value, the atmosphere collapses onto the polar caps. At low obliquities, the ability of the atmosphere to lift dust is greatly diminished (20), possibly providing an explanation for the radar observations. Obviously, the CO₂ now buried in RFZ₃ was in the atmosphere at some time in the past. A plausible assumption is

that the RFZ₃ mass was largely in the atmosphere when the insolation at the south pole at summer solstice was at a maximum, which for the past one million years occurred about 600,000 years ago [obliquity = 34.76°, eccentricity = 0.085, longitude of perihelion = 259.4° (21)].

To assess the impact on some first-order climate parameters, we ran a fast version of the NASA/Ames Mars GCM (version 1.7.3) for these orbital conditions with a total exchangeable CO₂ inventory (atmosphere plus caps) equal to the present inventory (7.1 mbar) plus 5 mbar. We found that most of the additional 5 mbar of CO₂ ended up in the atmosphere. Surface pressures rose uniformly around the planet, with global-mean annually averaged pressures equaling 10.5 mbar. Annual mean cap masses increased by about 0.8 mbar, not accounting for the lost RFZ₃ mass. Surface temperatures, however, decreased slightly (~0.7 K) because the CO₂ ice was on the ground for a longer period, and this compensated the modest greenhouse effect.

There are two implications of these changes in the climate system. First, the increased CO₂ pressure expands the geographic locations where these pressures exceed the triple-point pressure of water, thereby permitting liquid water to persist without boiling (although it may still evaporate, as on Earth) (22). Second, higher surface pres-

ures will lead to higher surface wind stresses, which will loft more dust in the atmosphere, leading to an increase in dust storm frequency and intensity. Given the complex interplay between the dust, water, and CO₂ cycles, additional changes in the climate system are very likely.

References and Notes

1. B. M. Jakosky, R. J. Phillips, *Nature* **412**, 237 (2001).
2. R. B. Leighton, B. C. Murray, *Science* **153**, 136 (1966).
3. P. C. Thomas, P. B. James, W. M. Calvin, R. Haberle, M. C. Malin, *Icarus* **203**, 352 (2009).
4. H. Kieffer, *J. Geophys. Res.* **84**, 8263 (1979).
5. S. Byrne, A. P. Ingersoll, *Science* **299**, 1051 (2003).
6. R. Seu *et al.*, *J. Geophys. Res.* **112**, E05505 (2007).
7. R. J. Phillips *et al.*, *Science* **320**, 1182 (2008); 10.1126/science.1157546.
8. N. E. Putzig *et al.*, *Icarus* **204**, 443 (2009).
9. R. Seu *et al.*, *Science* **317**, 1715 (2007).
10. Materials and methods are available as supporting material on Science Online.
11. E. Pettinelli *et al.*, *J. Geophys. Res.* **108**, 8029 (2003).
12. R. Simpson, B. Fair, H. Howard, *J. Geophys. Res.* **85**, 5481 (1980).
13. D. C. Nunes, R. J. Phillips, *J. Geophys. Res.* **111**, E06521 (2006).
14. E. J. Kolb *et al.*, "The residual ice cap of Planum Australe, Mars: New insights from the HRSC experiment." Paper presented at the 37th Lunar and Planetary Science Conference, League City, TX, 13 to 17 March 2006; www.lpi.usra.edu/meetings/lpsc2006/pdf/2408.pdf.
15. K. L. Tanaka, E. Kolb, C. Fortezzo, "Recent advances in the stratigraphy of the polar regions of Mars." Paper presented at the Seventh International Conference on

Mars, Pasadena, CA, 9 to 13 July 2007; www.lpi.usra.edu/meetings/7thmars2007/pdf/3276.pdf.

16. RFZ₃ is seen discontinuously in radargrams here, but key reflectors could not be mapped with high confidence likely because of surface scattering interference, resolution limitations, and lack of coverage.
17. A lower value of ~4000 to 4500 km³ is obtained with the unlikely assumption that RFZ₃ does not extend beyond SHARAD's data gathering locales, which are limited by MRO's orbital inclination. See (10).
18. R. C. Weast, *CRC Handbook of Chemistry and Physics* (CRC Press, Boca Raton, FL, ed. 55, 1974).
19. C. Newman, S. Lewis, P. Read, *Icarus* **174**, 135 (2005).
20. R. M. Haberle, J. R. Murphy, J. Schaeffer, *Icarus* **161**, 66 (2003).
21. J. Laskar *et al.*, *Icarus* **170**, 343 (2004).
22. R. Haberle *et al.*, *J. Geophys. Res.* **106**, 23317 (2001).

Acknowledgments: K. Herkenhoff and C. Fortezzo provided useful comments on an earlier version of the paper. Remarks by three anonymous referees were exceedingly helpful. Funding for this work was provided by the NASA MRO project. The radar and imaging data are available through NASA's Planetary Data System.

Supporting Online Material

www.sciencemag.org/cgi/content/full/science.1203091/DC1
Materials and Methods
SOM Text
Figs. S1 to S5
Tables S1 to S4
References

20 January 2011; accepted 23 March 2011
Published online 21 April 2011;
10.1126/science.1203091

Late Mousterian Persistence near the Arctic Circle

Ludovic Slimak,^{1*} John Inge Svendsen,² Jan Mangerud,² Hugues Plisson,³ Herbjørn Presthus Heggen,² Alexis Brugère,⁴ Pavel Yurievich Pavlov⁵

Palaeolithic sites in Russian high latitudes have been considered as Upper Palaeolithic and thus representing an Arctic expansion of modern humans. Here we show that at Byzovaya, in the western foothills of the Polar Urals, the technological structure of the lithic assemblage makes it directly comparable with Mousterian Middle Palaeolithic industries that so far have been exclusively attributed to the Neandertal populations in Europe. Radiocarbon and optical-stimulated luminescence dates on bones and sand grains indicate that the site was occupied during a short period around 28,500 carbon-14 years before the present (about 31,000 to 34,000 calendar years ago), at the time when only Upper Palaeolithic cultures occupied lower latitudes of Eurasia. Byzovaya may thus represent a late northern refuge for Neandertals, about 1000 km north of earlier known Mousterian sites.

Most of the Russian Arctic was free of glacier ice throughout the past 50,000 years, including during the Last Glacial Maximum (LGM) (1). A varied herbivorous fauna existed in high Arctic areas that are presently wet tundra or almost barren Arctic deserts (2). Recent archaeological evidence demonstrates that Ice Age humans also at least temporarily lived and hunted in these northern landscapes beginning around 35,000 to 36,000 ¹⁴C years before the present (yr B.P.) [≥40,000 yr B.P. in calibrated/calendar (cal) years] (3–7) (fig. S1). It has not been clear whether the early visitors were members of a fossil population [such as *Homo sapiens neanderthalensis* and affiliated groups

(8, 9)] or whether modern humans (*H. sapiens sapiens*) expanded northward into a previously uninhabited area.

This question is related to the Middle Palaeolithic (MP) to Upper Palaeolithic (UP) cultural transition in Eurasia. This transition, which has been considered to have taken place about 40,000 to 37,000 yr B.P. in most of Eurasia, saw the global extinction of the Neandertals and thus the end of their specific MP (Mousterian) culture. The Neandertals were replaced by modern humans, who were the bearers of all known UP cultures.

Here we describe lithic technology and age constraints from the Byzovaya site near the Polar Urals and show that humans bearing MP stone

technology persisted to 32,000 to 34,000 cal yr B.P. in the Eurasian Arctic (Fig. 1). Byzovaya, which is among the northernmost known Palaeolithic sites, was previously considered to be an Early Upper Palaeolithic (EUP) site mainly on the basis of a few radiocarbon dates that suggested an age of about 27,000 ¹⁴C years or younger.

The Byzovaya site (65°01'25"N, 57°25'12"E) is located on the right bank of the Pechora River, which flows northward across the lowland areas west of the Ural Mountains (Fig. 1). First described in 1965 by Guslitsier *et al.* (10), the locality was investigated several times by Russian archaeologists (11); later by a Norwegian-Russian team, since 1996 (6, 12); and by a French-Russian team since 2007. More than 300 stone artefacts and 4000 animal remains have been uncovered during the various excavations, which together cover an area of approximately 550 m².

¹CNRS, UMR 5608, TRACES, Université de Toulouse le Mirail, Maison de la Recherche, 5 Allées Antonio Machado, 31058 Toulouse Cedex 9, France. ²Department of Earth Science and Bjerknes Centre for Climate Research, University of Bergen, Allégaten 41, N-5007, Bergen, Norway. ³CNRS, UMR 5199, PACEA, IPGQ, Université Bordeaux 1, Bâtiment B18, Avenue des Facultés, 33405 Talence Cedex, France. ⁴CNRS, USR 3225 and UMR 7041, ArScAn, "Archéologies Environnementales," Maison de l'Archéologie et de l'Ethnologie René Ginouvès, CC023, 21, Allée de l'Université, 92023 Nanterre Cedex, France. ⁵Department of Archaeology, Institute of Language, Literature and History, Komi Science Centre, Russian Academy of Sciences, Kommunisticheskaya Street 26, 167000 Syktyvkar, Komi, Russia.

*To whom correspondence should be addressed. E-mail: slimak@univ-tlse2.fr